Tectonophysics 609 (2013) 547–557

Contents lists available at ScienceDirect

Tectonophysics

journal homepage: www.elsevier.com/locate/tecto

Review Article

The Moho in subduction zones

M.G. Bostock *

Department of Earth and Ocean Sciences, The University of British Columbia, Vancouver, British Columbia, Canada

ARTICLE INFO

Article history:
Received 25 February 2012
Received in revised form 27 June 2012
Accepted 7 July 2012
Available online 26 July 2012

Keywords:
Subduction zone
Low velocity zone
Mantle forearc serpentinization
Metamorphic dehydration

ABSTRACT

The Moho in subduction zones exists in two distinct forms, one associated with the subducting oceanic plate and second with the overriding plate. The seismic expression of both forms is linked to the nature of a landward dipping, low-velocity zone (LVZ) that has been detected in a majority of subduction zones about the globe and that approximately coincides with Wadati–Benioff seismicity. We review seismic studies that constrain the properties of the LVZ in Cascadia where it has been extensively studied for over a quarter century. A model in which the LVZ is identified with hydrated pillow basalts and sheeted dikes of oceanic crustal Layer 2, is consistent with available geological and geophysical data, and reconciles previously conflicting interpretations. In this model, the upper oceanic crust is hydrated through intense circulation at the ridge and becomes overpressured upon subduction as a result of metamorphic dehydration reactions combined with an impermeable plate boundary above and a low porosity gabbroic Layer 3 below. The resulting seismic velocity contrast (approaching 50% for *S*-waves) significantly overwhelms that of a weaker, underlying oceanic Moho. At greater depths, oceanic crust undergoes eclogitization in a top-down sense leading to gradual disappearance of the LVZ. The large volume change accompanying eclogitization is postulated to rupture the plate boundary allowing fluids to penetrate the cooled, forearc mantle wedge. Pervasive serpentinization and free fluids reduce velocities within the wedge, thereby diminishing, erasing or even inverting the seismic contrast associated with the Moho of the overriding plate. This model is tested against observations of LVZs and forearc mantle structure worldwide.

Contents

1. Introduction

Subduction zones are critical junctures in the Earth's geological evolution where crust is created, consumed and recycled. Given this concentration of geological activity, it is expected that a variety of processes may act to perturb the crust–mantle boundary (hereafter referred to as "Moho") and/or modify its seismic expression. The nature of subduction zones implies the convergence of two plates, each characterized by a distinct Moho: one Moho associated with the incoming oceanic plate and another that may be of either continental or oceanic affinity. In this paper, we shall examine the processes operating in subduction zone forearcs that influence the elastic properties of both subducting and overriding plates with specific reference to their respective Mohos. Our focus will be largely directed to information recovered

* Department of Earth and Ocean Sciences, The University of British Columbia, 2219 Main Mall, Vancouver, BC V6T 1Z4, Canada. Tel.: +1 604 822 2082.
E-mail address: bostock@eos.ubc.ca.

0040-1951/$ – see front matter © 2012 Elsevier B.V. All rights reserved.
http://dx.doi.org/10.1016/j.tecto.2012.07.007

using scattered teleseismic waves, although we shall also draw on relevant evidence from active sources, tomographic and other geophysical studies where applicable.

The following treatment is divided into two parts. In the first part, we consider the Cascadia subduction zone which ranks among the best studied subduction zones worldwide, and for which a consistent model is emerging for the interaction of the two plates and its influence on their crustal signatures. This model implies that water plays a prominent role in dictating the expression of both Mohos from trench to arc. In the second part, we will review results from other subduction zones in light of this model, evaluate its general applicability and discuss some of the resulting implications.

2. Cascadia

Cascadia is a warm subduction zone, extending over 1000 km from northern California to northern Vancouver Island (see Fig. 1), that has been extensively investigated using both active and passive source seismology. Structures below 100 km depth have been characterized primarily by using teleseismic traveltime tomography (e.g., Audet et al., 2008; Bostock and VanDecar, 1995; Michaelson and Weaver, 1986; Obrebski et al., 2010; Rasmussen and Humphreys, 1988; Schmandt and Humphreys, 2011) and will not be further considered here. The detailed expressions of oceanic and continental crusts at shallower levels in the forearc region, in particular beneath southwestern British Columbia and adjacent Washington State, have been illuminated through a combination of seismic reflection imaging, receiver function analysis and regional body wave tomography, each with different sensitivity to structure and physical properties (see Fig. 2 for a schematic diagram of seismic experimental geometries used to interrogate shallow subduction zone structure). Since the earliest receiver function studies (Langston, 1977, 1981), it has been apparent that forearc structure is dominated by the presence of a landward-dipping, low-velocity zone (LVZ) (see Fig. 3). This feature is now known to span the entire Cascadia margin from the coast to a depth of at least 45 km below the forearc basins (Georgia Strait, Puget Sound, Willamette Valley; see Audet et al., 2010; Nikulin et al., 2009). It coincides with a zone of high seismic reflectivity and electrical conductivity where active source (Clowes et al., 1987a; Green et al., 1986; Hyndman et al., 1990) and magnetotelluric surveys (Kurtz et al., 1990; Soyer and Unsworth, 2006; Wannamaker et al., 1989) have been undertaken, and is referred to as the "E"-layer on the southern Vancouver Island Lithoprobe transect. The LVZ must be placed in a proper geometrical and petrological context within the subduction zone in order to appreciate variations in the seismic expression of the Moho in this region.

The incoming Juan de Fuca plate is clearly imaged on a number of offshore marine seismic profiles (e.g. Clowes et al., 1987b; Nedimovic et al., 2009) through reflections from the sediment basement contact and a weaker Moho reflection following approximately 2 s later. This signature is more difficult to trace landward of the deformation front due, at least in part, to the large lateral velocity contrasts that characterize sediments in the accretionary prism (e.g., Hyndman et al., 1990; Nedimovic et al., 2003; see Fig. 4). As a consequence, it is a non-trivial exercise to tie the incoming Moho to structures on the adjacent land-based Lithoprobe reflection profiles. Indeed, some early interpretations of seismic reflection (Green et al., 1986) and receiver function (Langston, 1981) data identified the LVZ (or high reflectivity E-layer) as oceanic crust, whereas other more recent considerations of both

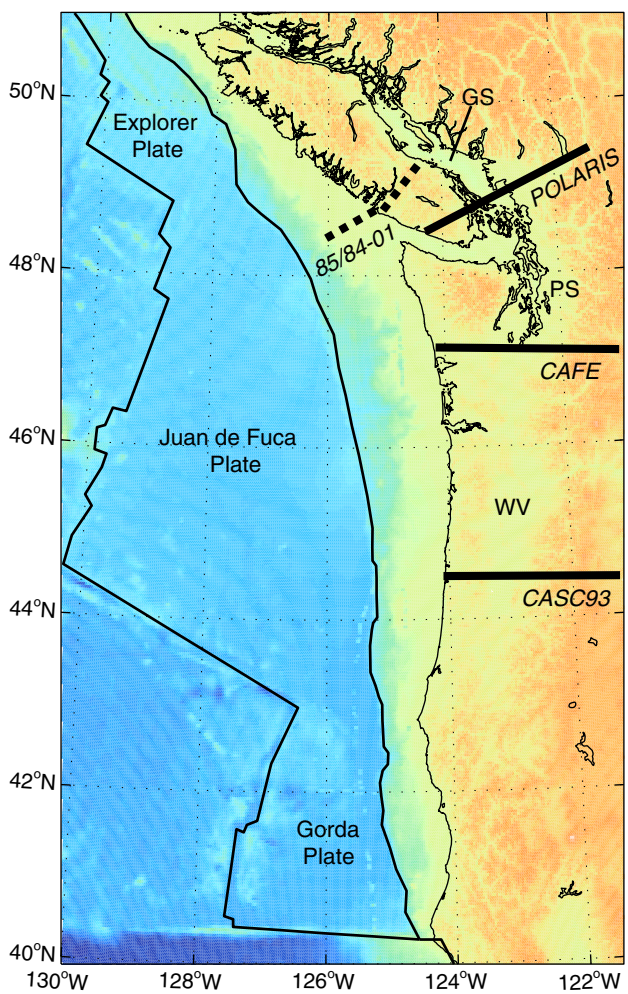

Fig. 1. Bathymetric/topographic map of Cascadia subduction zone. Forearc lowlands are labelled as GS (Georgia Strait), PS (Puget Sound) and WV (Willamette Valley). Approximate locations of POLARIS, CAFE and CASC93 teleseismic profiles, plotted in Fig. 5, are shown in black solid lines. The approximate location of the combined marine (85–01) and land (84–01) profiles shown in Fig. 4, is plotted as a dashed line.

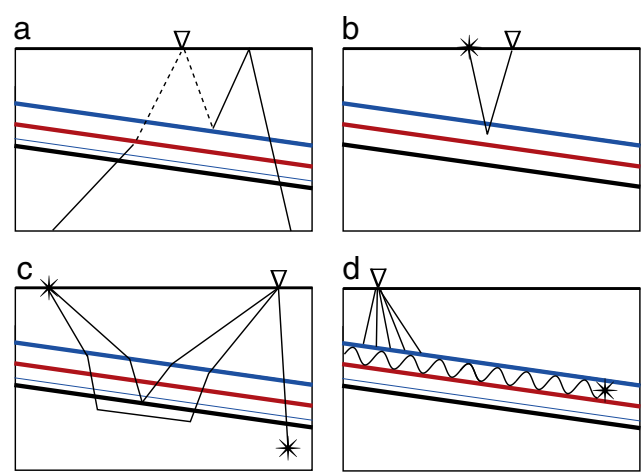

Fig. 2. Ray geometries employed in seismic studies that interrogate shallow subduction zone structure. Upper and lower boundaries of dipping low velocity zone (LVZ) are shown as blue and red lines, respectively; oceanic Moho, as interpreted in this study, underlies LVZ and is shown as a thick black line. Star and inverted triangle denote the source and receiver, thin lines mark *P*-rays (solid) and *S*-rays (dashed). a) Receiver functions employ low-frequency (0.1–1.0 Hz) teleseismic body waves to illuminate LVZ structure through conversions and free-surface reverberations at its upper and lower boundaries. b) Seismic reflection studies employing higher frequencies (10–50 Hz) image the LVZ as a layer exhibiting strong internal reflectivity. c) Refraction seismic tomography has reduced sensitivity to LVZ but can detect underlying oceanic Moho through head waves and post-critical reflections. Inclusion of earthquake sources below the LVZ within tomographic studies improves sensitivity to LVZ structure. d) Guided wave studies exploit waves channelled up the LVZ from earthquake sources at depths that lie within it. Heterogeneous structure at shallower levels allows dispersed guided waves to leak from the LVZ to receivers at the surface.

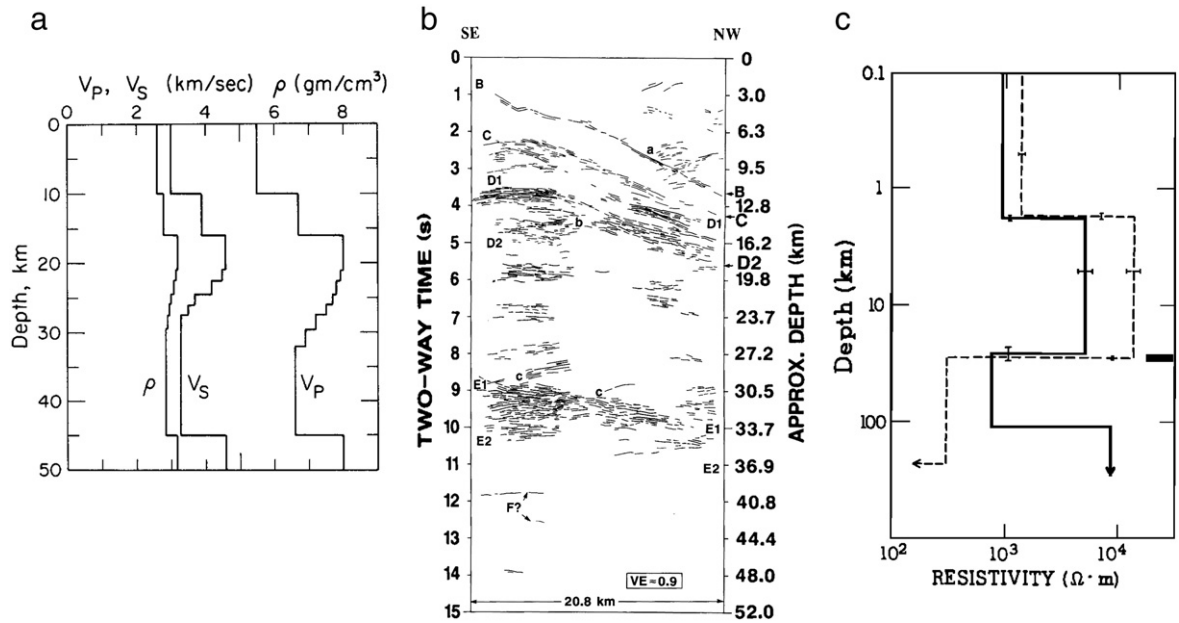

Fig. 3. Early documentation of the LVZ. a) Velocity model from Langston (1977) displaying pronounced LVZ recovered from receiver functions using long period WWSSN recordings recorded at Corvallis, Oregon. b) Line drawing from Lithoprobe reflection line 4 (Clowes et al., 1987a); the LVZ coincides with the high reflectivity E-layer delimited by symbols E1 and E2. c) Resistivity-depth model for central Vancouver Island showing low resistivity (high conductivity) associated with E-layer/LVZ (Kurtz et al., 1990).

active and passive seismic data (e.g., Calvert and Clowes, 1990; Cassidy and Ellis, 1993; Hyndman et al., 1990) have placed the top of the downgoing plate 5–10 km below the LVZ. These latter interpretations of plate boundary location have appealed to velocity structures determined from seismic refraction and tomographic studies based on standard reference models, and to the assumption that Wadati–Benioff seismicity reside within the oceanic crust.

Recent receiver function studies have drawn attention to the extreme elastic properties that characterize the LVZ. Audet et al. (2009) exploited differential times of direct conversions and free-surface reverberations to demonstrate that Poisson's ratios internal to the LVZ beneath southern Vancouver Island are unusually high, $\sigma = 0.40$. On the basis of rock physical measurements such values cannot be attributed to lithology alone but must involve high pore fluid pressures (Christensen, 1984, 1996). Furthermore, *S*-velocities must be very low (50–70% those of bounding layers) and the true thickness of the LVZ/E-layer, of order 4 km, is rather less than previous estimates. Note that standard imaging schemes employing reference models and regularization to map wave arrival times to depth (e.g. tomography, migration) will tend to overestimate LVZ thickness and underestimate its velocity contrast. Values for LVZ thickness, velocity contrast and Poisson's ratio made by Audet et al. (2009) below southern Vancouver Island have been corroborated and extended to stations along the entire Cascadia margin using receiver function waveform inversion of both direct conversions and reverberations by Hansen et al. (2012). These authors also demonstrate the ubiquity of a second, less prominent, underlying layer with a more typical Poisson's ratio ($\sigma \sim 0.29$) but with comparable thickness. Taken in combination, the LVZ and underlying layer have a total thickness of 8 km and, upon consideration of constraints from studies of ophiolites (e.g., Salisbury and Christensen, 1978; Salisbury et al., 1989), oceanic crustal permeability (Fisher, 1998) and in situ velocity measurements (Rohr, 1994), have been collectively interpreted as subducted oceanic crust. More specifically, the layering is considered in terms of the classic divisions of oceanic crust as determined from seismic refraction studies, e.g. Raitt (1963), Christensen and Salisbury (1975), White et al. (1992). The LVZ is identified with pervasively hydrated, high porosity, pillow basalts and sheeted dikes of Layer 2 with possible contributions from marine sediments (Layer 1). The underlying layer is represented by a low porosity, gabbroic Layer 3 with much lower degrees of hydration. High pore fluid pressures are maintained in Layer 2 (±Layer 1) through a low porosity Layer 3 below and an impermeable plate boundary seal above.

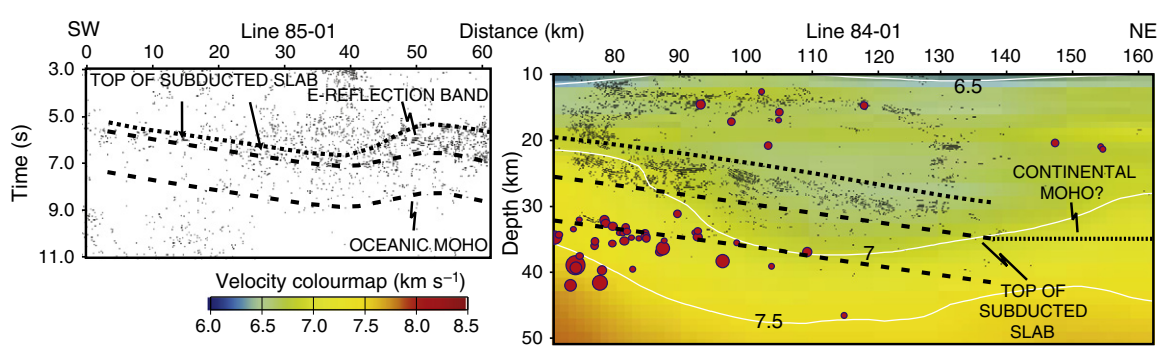

Fig. 4. Composite seismic reflection dip-profile across southern Vancouver Island from Nedimovic et al. (2003). Line drawings are time migrated stacks that reveal evolution of the simple top of subducting plate offshore (SW) into the complex zone of high reflectivity (E-zone) below Vancouver Island (NE). The original study mapped the top of slab plate into the base of the E-layer whereas the current model traces this feature into the top of the E-layer. Note the ~1 s pull-up structure between 40 and 50 km distance produced by large velocity change at the boundary between Eocene the fossil trench and Pacific Rim terrain.

The latter structure may be generated through grain size reduction, mineral precipitation from migrating fluids or volume expanding metamorphic hydration reactions (Peacock et al., 2011).

At a depth of approximately 45 km, the LVZ begins to lose its prominent signature, and the reduction in strength appears to occur progressively in a top-to-bottom sense (Rondenay et al., 2001). Once more, this behaviour persists along strike of the entire Cascadia margin with an along-dip onset corresponding to the major forearc depressions (Georgia Strait, Puget Sound, Willamette Valley, see Fig. 1). The signal is effectively lost by ~100 km depth below Puget Sound and the Willamette Valley (Abers et al., 2009; McGary et al., 2011; Nabelek et al., 1996; Rondenay et al., 2001) and possibly at shallower levels beneath southern Vancouver Island (Nicholson et al., 2005) as shown in Fig. 5. The reduction in seismic velocity contrast of the LVZ has been attributed in these studies to the effect of eclogitization that is expected to initiate in metabasalts at the top of oceanic crust, where temperatures are highest, and spread progressively (perhaps kinetically hindered) into coarser grained gabbros as subduction proceeds, and temperatures and pressures increase (Hacker et al., 2003b). Eclogitization reduces the seismic velocity contrast within the LVZ in two ways. First, mineralogy changes with, for example, lower-velocity plagioclase–pyroxene assemblages replaced by higher-velocity garnet–pyroxene assemblages, resulting in a lithology that has composite elastic properties similar to those of upper mantle

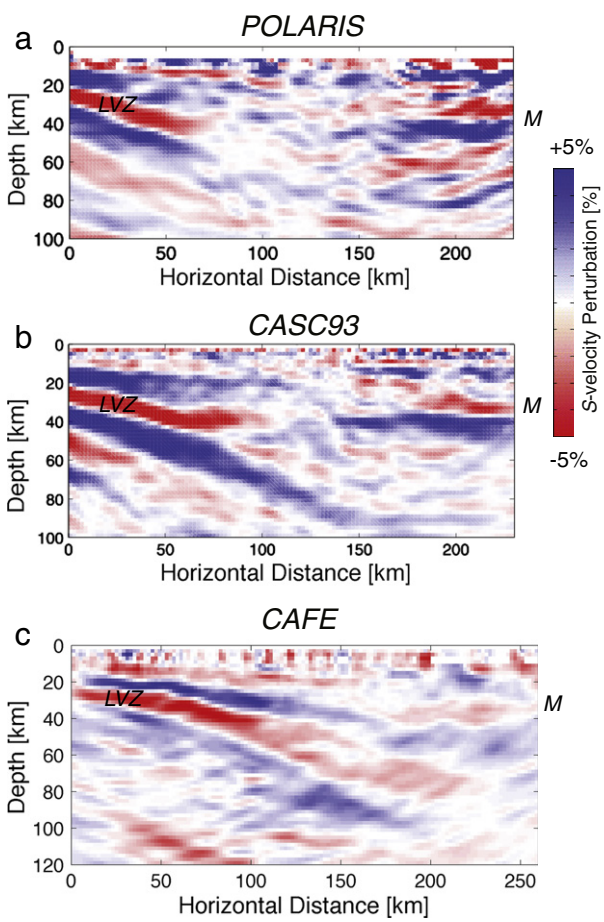

Fig. 5. Scattered wave images of *S*-velocity structure taken from 3 studies across a) southern Vancouver Island (POLARIS, Nicholson et al., 2005); b) central Oregon (CASC93, Nabelek et al., 1996; Rondenay et al., 2001); and c) Puget Sound (CAFE, McGary et al., 2011; Abers et al., 2009). Locations of 3 profiles are indicated in Fig. 1. The LVZ (dipping "red" layer) is labelled on each profile. An "M" at the eastern end of the profiles marks the depth of the continental Moho that separates low-velocity (red) crust from high-velocity (blue) mantle. In each case, this Moho disappears seaward beneath the forearc mantle wedge.

peridotite under dry conditions (Christensen, 1996). Second, and just as importantly, eclogitization produces an ~10% volume reduction in the solid phase (and a concomitant production of free water, e.g., in Hacker (1996)) that is postulated to compromise the plate boundary seal developed at shallower levels, thereby reducing pore pressures and enabling hydrous fluids to escape into the mantle wedge (Audet et al., 2009).

Introduction of fluids into a forearc mantle wedge of peridotitic composition that is cooled by the presence of the subducting plate is expected to produce dramatic changes in mineral composition and elastic properties (Hyndman and Peacock, 2003). In particular, hydration of peridotite at temperatures under 600° at pressures near 1.0 GPa leads to formation of antigorite (Peacock and Hyndman, 1999; Ulmer and Tromsdorff, 1995), a high temperature serpentine mineral characterized by elastic wave velocities that fall significantly below those of peridotite (Christensen, 2004). In fact, the effect is sufficient to render velocities in the mantle wedge comparable to those of lower crustal lithologies, producing a simple, seismically testable hypothesis for the presence of a serpentinized forearc mantle, namely the absence of a seismically defined forearc Moho defining the base of the continental crust. This hypothesis has been tested in several studies in Cascadia using active and passive seismic data. Bostock et al. (2002) noted the progressive disappearance and inversion of the continental Moho seaward of the volcanic arc to the wedge corner on a migrated receiver function profile across central Oregon. Migrated receiver function profiles across southern Vancouver Island (Nicholson et al., 2005) and Puget Sound (Abers et al., 2009) also reveal an absence of continental Mohos in the forearc region, although there is no Moho inversion nearing the wedge corner on these profiles (Fig. 5). The magnitude of velocity reduction implied by a Moho inversion (that is, a seismic velocity contrast where high velocity, lower continental crust is juxtaposed against low-velocity, underlying mantle) cannot originate through antigorite serpentinization alone, but likely requires the additional presence of fluids at high pore pressures and/or significant contributions from other hydrous minerals, e.g., chlorite (Christensen, 2004). Extensive fracturing might be expected within the mantle wedge given the ~20% volume increase associated with antigorite hydration (Coleman, 1971). The receiver function results are supported by a compilation of seismic refraction profiles along the Cascadia margin analysed by Brocher et al. (2003), all of which indicate an absence of the P_MP phase (and, accordingly, continental Moho) in the Cascadia forearc. Further supporting evidence for forearc serpentinization in Cascadia is afforded through regional tomographic models (Ramachandran et al., 2006; Zhao et al., 2001), and potential field anomalies that indicate low-density and strongly magnetic signatures where seismic Moho is absent (Blakely et al., 2005). This latter material property combination is unusual, but can be explained by a forearc mantle wedge comprising large quantities of antigorite which, although of low density, forms along with magnetite during hydration of peridotite (Saad, 1969).

Fig. 6, taken from Hansen et al. (2012) summarizes the various processes described above and that are considered here to be key in controlling the seismic expression of oceanic and continental crusts and, in particular, their respective Mohos, in Cascadia:

i) upper oceanic crust comprising pillow basalts and sheeted dikes is intensely hydrated through vigorous hydrothermal circulation at the Juan de Fuca ridge;
ii) as ocean spreading proceeds, sediments carpet the ocean bottom, the plate cools, and free water is incorporated within hydrous minerals;
iii) additional hydration may take place along new and reactivated faults in the trench/outer-rise region (e.g. Peacock, 2001);
iv) upon subduction, increased temperatures and pressures cause prograde metamorphic dehydration reactions to commence and produce hydrous fluids at near lithostatic pore-fluid pressures

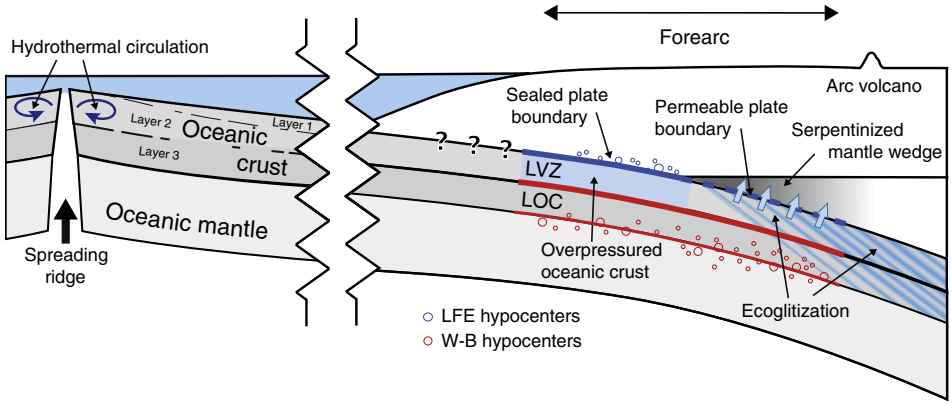

Fig. 6. Schematic model illustrating hydrologic evolution of ocean crust in Cascadia, from Hansen et al. (2012). Vigorous hydrothermal circulation near oceanic ridge results in pervasive hydration, preserved as hydrous minerals, in a porous Layer 2. Upon initiation of subduction, metamorphic dehydration reactions (±compaction) commence to produce free fluids at near-lithostatic pressures within Layer 2 (±Layer 1). Pressure is maintained by an impermeable plate boundary above, and a nonporous Layer 3 (LOC) below, resulting in high Poisson's ratio for the LVZ. Eclogitization commences near 45 km depth and is accompanied by a ~10% volume change that compromises the plate boundary seal and initiates serpentinization of the mantle wedge. A top to down loss of the LVZ then occurs with increasing depth. Inferred hypocentral locations of low frequency (LFE) and Wadati–Benioff (W-B) earthquakes are indicated in blue and red circles, respectively.

(Fyfe et al., 1978) that are maintained within the upper oceanic crust by an impermeable plate boundary above and a massive and largely impermeable gabbroic/cumulate lower crust below. The effect of high pore pressures in the upper oceanic crust (and possibly overlying sediments) dominates elastic property contrasts creating a prominent LVZ that considerably overwhelms the contrast associated with underlying oceanic Moho;

v) metamorphic reactions culminate near 45 km depth with the onset of eclogitization, as predicted from thermo-petrological models, liberating remaining fluids and causing volumetric changes capable of rupturing the plate boundary seal;

vi) hydrous fluids penetrate a cooled mantle wedge leading to extensive serpentinization and fracturing, and an erasure of the seismic contrast with overlying continental crust, that is, the continental Moho;

vii) eclogitization proceeds in a top-down manner, beginning with metabasalt and progressing into coarser grained, gabbroic material at greater depths, with eclogitization largely completed by 100 km depth.

There are two general conclusions that can be drawn from this model (hereafter referred to as the "current" model). First and foremost, water plays a major role in governing the seismic expression of various crustal and mantle elements within the Cascadia subduction zone complex. Second, the effect of water is to reduce the seismic expression of the two Mohos. In studies employing scattered waves (seismic reflection profiling, receiver functions), the signature of the oceanic Moho is largely overshadowed by that of an overpressured upper oceanic crust, roughly 4 km above, displaying strongly reduced velocity, increased Poisson's ratio and pervasive, high amplitude reflectivity (note that wide angle reflections observed in active source refraction profiles (e.g., Trehu et al., 1994; Parsons et al. (1998); Preston et al., 2003) are less influenced by LVZ structure and thereby afford a less ambiguous detection of oceanic Moho, see Fig. 2c). Seismic expression of the continental Moho in the forearc region is reduced to greater or lesser degrees by serpentinization and the presence of free water in the mantle wedge. In some instances, their combined effect may be sufficient to produce an inverted Moho juxtaposing high velocity crust with low-velocity mantle.

3. Reconciliation with previous interpretations

Prior to proceeding to more general discussion concerning expression of the Moho in subduction zones globally, it is worth recounting previous models of plate structure in Cascadia and summarizing how the current model affects conclusions drawn from these earlier studies. The essential differences between the 5 models are indicated schematically in Fig. 7.

Model A: *LVZ/E-layer is identified with the oceanic crust in its entirety* (Audet et al., 2009, 2010; Bostock et al., 2002; Green et al., 1986; Langston, 1981; Nicholson et al., 2005). In the current model, the LVZ represents only the upper half of the oceanic crust, and hence location of the oceanic Moho is shifted approximately 4 km below that inferred in these earlier studies, rendering it generally consistent with estimates from wide-angle reflections (e.g., Preston et al., 2003). Inferences regarding position of the plate boundary (Audet et al., 2010) and physical properties (thickness, permeability, porosity) of the LVZ (Peacock et al., 2011) remain unaffected. Some portion of the Wadati–Benioff seismicity previously inferred to occur in the uppermost mantle is now relocated within the lower oceanic crust.

Model B: *LVZ/E-layer represents a distributed shear zone forming an extended plate boundary* (Nedimovic et al., 2003). These authors employ data from both Lithoprobe and more recent SHIPS surveys to trace the top of plate continuously from offshore profiles, where the reflectivity is sharp, landward into the E-layer where it becomes distributed. They interpret the corresponding change in reflection character as caused by a change in the style of deformation from locked into transitional sliding along the plate boundary, but infer that oceanic crust lies at the base of the E-layer (see Fig. 4). Their observation of a continuous transition from the top of plate seaward into the E-layer landward is consistent with the current model except that, in the latter case, the top of plate merges into the top, rather than the bottom, of the E-layer. Moreover, an association between plate boundary deformational mode and structure remains through the requirement of high pore pressures (and resulting low normal stresses) in recently reported mechanisms of slow-slip genesis (Segall et al., 2010).

Model C: *LVZ/E-layer represents serpentinized material drawn into the plate boundary from the mantle wedge via slab rollback* (Nikulin et al., 2009; Park et al., 2004). This model was motivated by the observation that the LVZ displays both high Poisson's ratio (~0.33) and significant anisotropy as illuminated by receiver functions at select broadband stations beneath the Cascadia

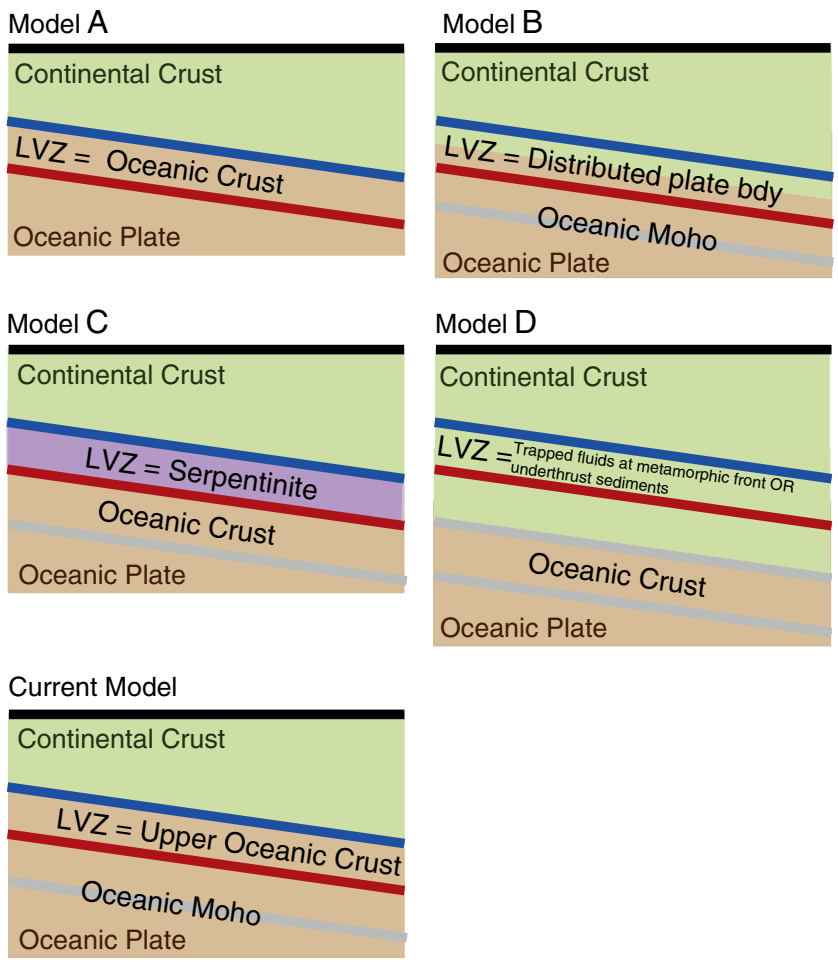

Fig. 7. Schematic models illustrating the 5 LVZ models considered in the text for the Cascadia forearc region. Model A identifies LVZ as subducting oceanic crust in its entirety (e.g. Nicholson et al., 2005; Audet et al., 2009); Model B invokes an interpretation of the LVZ as a distributed plate boundary (Nedimovic et al., 2003); Model C ascribes the LVZ to a layer of serpentinite drawn into the plate boundary from the mantle wedge (Park et al., 2004; Nikulin et al., 2009); Model D places the LVZ within the continental crust as the result of either retrograde metamorphic reactions (e.g. Hyndman, 1988) or sediment underthrusting (e.g. Calvert et al., 2011); the current model advocated in this paper identifies the LVZ with the upper oceanic crust as detailed in Fig. 6.

forearc. It possesses at least one critical flaw. Christensen (2004) has demonstrated that antigorite, the only serpentine mineral stable at temperatures corresponding to depths between 20 and 40 km, is characterized by markedly lower Poisson's ratios of 0.29. Furthermore, the anisotropic properties of antigorite from mantle assemblages are not yet fully understood. Although antigorite is a highly anisotropic mineral and a lab study of a sample containing 75% antigorite of unknown provenance has reported >20% anisotropy (Kern, 1993), a sample of 95% antigorite from Stonyford California displays only 2% anisotropy (Christensen, 1978; Hansen et al., 2012). Moreover studies of massive antigorite in outcrop from subduction zone assemblages in Cascadia indicate that foliations, when present are usually defined by magnetite and so unlikely to produce significant anisotropy (Brown et al., 1982; Peacock, 1987).

Model D: *LVZ/E-layer resides above the plate boundary within the overriding continental crust either as a fluid rich layer* (Hyndman, 1988) *or as underplated sediments* (Calvert and Clowes, 1990; Calvert et al., 2011). The former study invokes a scenario with some similarity to the current model, namely that the highly reflective and conductive E-layer represents fluids trapped below an impermeable boundary. In that study, however, the boundary represents a retrograde metamorphic front in the upper plate where lower temperature/pressure facies minerals precipitate. Accordingly, fluids are interpreted to have migrated into the continental crust from a dehydrating oceanic crust 5–10 km below the E-layer. The current model alleviates a key difficulty with this interpretation by identifying the E-layer directly with upper oceanic crust, thereby obviating the need for fluid concentrations far away from a seismically transparent fluid source.

The second model identifies the LVZ/E-layer plate with sediments that have been underplated to the continental crust through continuing subduction (Calvert and Clowes, 1990; Calvert et al., 2011). A number of objections can be raised to this interpretation. First, the studies of Audet et al. (2010) and Hansen et al. (2012) indicate that the LVZ is contiguous throughout the Cascadia forearc, displaying consistent thickness and seismic expression along ~1000 km of margin. Second, the LVZ/E-layer can be traced well into mantle depths. Receiver functions image low velocities to depths of up to 100 km, whereas high-reflectivity in seismic reflection profiles can in several instances be traced to depths of ~50 km (Calvert et al., 2006, 2011; Clowes, pers. comm.) with apparent depth extent potentially limited by depth

penetration of waves from surface sources. Further objection to this model will be raised in the following section, upon consideration of seismic responses in other subduction zones.

4. The global survey

In previous sections we have provided a comprehensive description of processes that control the seismic expression of crust, mantle and Moho in the forearc region of the Cascadia subduction zone. Our objective, now, is to further evaluate the viability of this model through its applicability to other subduction zones globally. We shall proceed by reviewing literature as it pertains to a set of 4 criteria, namely the geographical distribution of LVZ's, their thickness and elastic properties, their seismic expression in depth and evidence for forearc mantle serpentinization.

4.1. LVZ distribution

The increased availability of 3-component, broadband instrumentation has led to a large number of receiver function studies of subduction zones undertaken over the past decade. These studies include Alaska (Ferris et al., 2003; Rondenay et al., 2008), Honshu (Kawakatsu and Watada, 2007), Nankai (Abe et al., 2011; Kato et al., 2010; Shiomi et al., 2004, 2008), Mariana (Tibi et al., 2008), New Zealand (Boyd et al., 2007), Chile/Peru (Sodoudi et al., 2011; Yuan et al., 2000), Nicaragua and Costa Rica (MacKenzie et al., 2010), central (Kim et al., 2010, in press) and southern Mexico (Kim et al., 2011), Greece (Li et al., 2003; Suckale et al., 2009; Pearce et al., 2012) and Calabria (Agostinetti et al., 2009). In all of these regions, landward, dipping LVZs are observed to approximately coincide with Wadati–Benioff seismicity, and to possess seismic signatures generally comparable to those described for Cascadia (see Figs. 5 and 8).

In addition to receiver function analyses, LVZs have also been illuminated using regional tomography in Honshu (Tsuji et al., 2008; Zhang et al., 2004) and Nankai (Shelly et al., 2006), with regional and teleseismic body wave modelling in central Mexico (Song et al., 2009) and through analysis of dispersed, guided waves travelling paths along the slab in the Alaska, Aleutians, Kamchatka/Kuriles, Kuriles/Hokkaido, Marianas, Nicaragua (e.g. Abers, 2000, 2005) and Chile (Martin et al., 2003) subduction zones within the forearc and, in some cases, into the backarc. Large-scale active source seismic and magnetotelluric surveys have been undertaken in far fewer locations but also indicate correlations between high reflectivity (central Andes, Oncken and the ANCORP working group, 1999; Gross et al., 2008), high Poisson's ratios (southwest Japan, Kodaira et al., 2004) and high conductivity (southern Mexico, Jödicke et al., 2006).

It appears, therefore, that in virtually all subduction zones that have been interrogated with sufficient density of instrumentation, there exists a dipping LVZ that follows Wadati–Benioff seismicity within the forearc region. The model discussed in points i)–vi) of Section 2, naturally accounts for the ubiquitous nature of the LVZ through its origin within Layer 2 of the oceanic crust, an essential and integral component of all subducting plates. Given the range of incoming sediment budgets for the subduction zones listed above (Rea and Ruff, 1996), an origin for the LVZ as underplated sediments as in model C of Section 3 would seem improbable.

4.2. LVZ thickness and elastic properties

In most of the aforementioned receiver function studies, thicknesses and velocities have been estimated using delay times of direct *P*-to-*S* conversions from the top and bottom of the LVZ, and mapped to depths using background velocity models. It is widely appreciated that, in this case, pronounced trade-offs exist between thicknesses and Poisson's ratio of layering (Zhu and Kanamori, 2000). Thickness

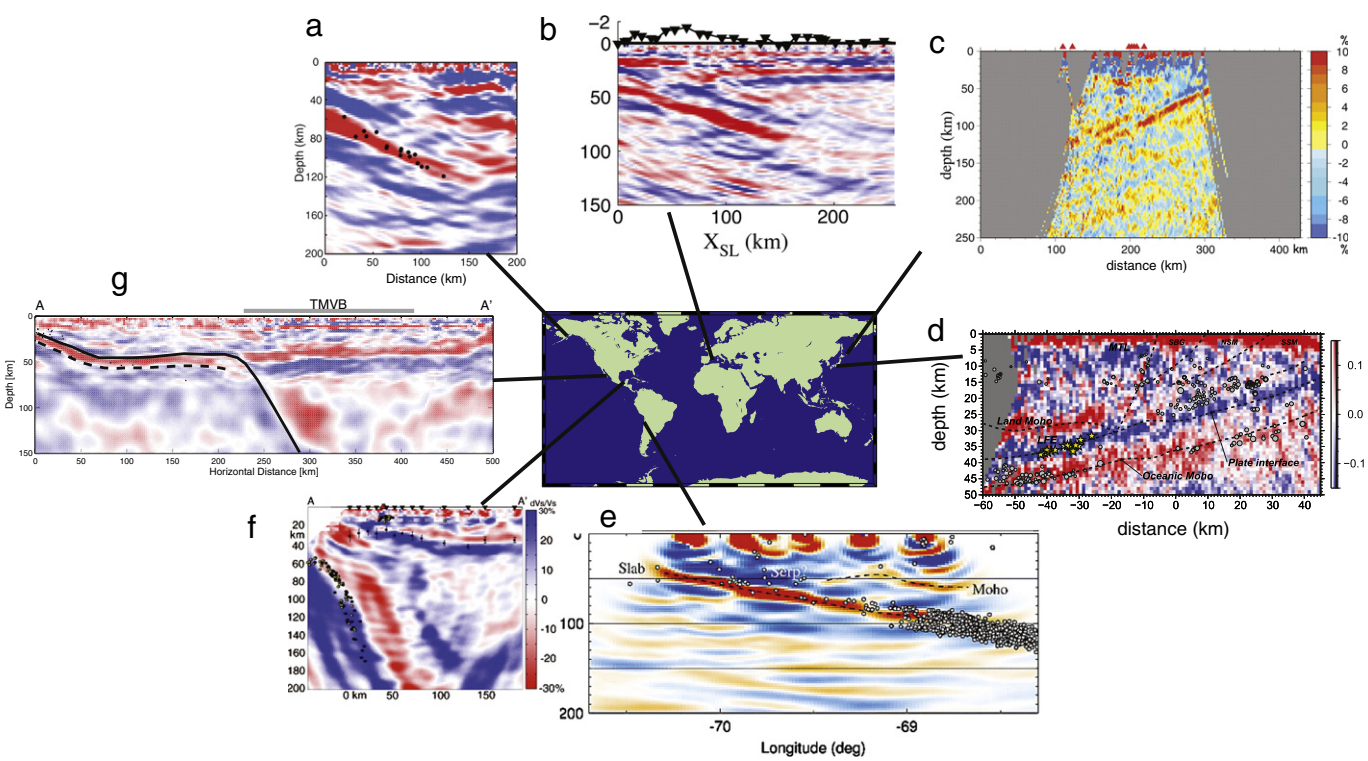

Fig. 8. A selection of teleseismic images of subduction zones representing contrasting thermal regimes and geometries all of which reveal the presence of a pronounced LVZ near the top of the subducting plate: a) Alaska (Rondenay et al., 2008), b) Greece (Pearce et al., 2012), c) Honshu (Kawakatsu and Watada, 2007), d) Nankai (Kato et al., 2010), e) central Andes (Sodoudi et al., 2011), f) Central America (MacKenzie et al., 2010); and g) Central Mexico (Kim et al., in press). Note that images in a, b, f and g show *S*-velocity perturbations and so the LVZ is defined as a dipping, negative velocity (red) perturbation layer. Images in c–e display "reflectivity" where the top and bottom of the LVZ are evident as negative (blue) and positive (red) polarity signals, respectively.

estimates are, accordingly, only as accurate as knowledge of background Poisson's ratio. If background Poisson's ratios are biased low, for example $\sigma = 0.30$ (dry basalt, Christensen (1996)) versus $\sigma = 0.40$ (as measured for Cascadia), then LVZ thickness will be overestimated by a factor of up to 70%. Consequently, LVZ thicknesses quoted from receiver function studies that employ direct *P*-to-*S* conversion traveltimes alone must be viewed as upper limits. Note that in Cascadia receiver function analyses, the LVZ thickness versus σ trade-off is resolved through inclusion of reverberations within either stacking procedures (Audet et al., 2010) or nonlinear waveform inversion (Hansen et al., 2012).

Regional body wave tomography can be used to better constrain velocity structure of LVZs. The high station density in Japan afforded through Hi-Net probably allows the best resolution of subduction zone velocity structure anywhere on the planet. Double difference tomography yields striking images of the LVZ in the subducting Pacific plate of northwest Japan (Tsuji et al., 2008) that document elevated Poisson's ratios ($\sigma \sim 0.35$). Studies of the Philippine Sea plate in southwest Japan using the same technique (Shelly et al., 2006) and active source refraction profiling (Kodaira et al., 2004) also indicate that the top of the plate is characterized by high Poisson's ratios ($\sigma = 0.30 - 0.34+$) as it approaches the mantle wedge. Moreover, it is important to appreciate that velocity images recovered from traveltime inversion are almost certainly biased toward background values, owing to i) regularization required to stabilize the inverse problem, ii) inherent difficulties in imaging low velocity zones with surface sources (Gerver and Markushevitch, 1966) and more generally (Wielandt, 1987), iii) earthquake relocation (for passive source studies). The general effect is nicely illustrated by Song and Helmberger (2007) who demonstrate that tomographic velocity models (produced from teleseismic traveltimes) can be used to generate synthetic seismograms that closely match observed waveforms, but only after amplification of velocity anomalies by 200–300%. Thus, the LVZ Poisson's ratios reported in studies employing refraction tomography should be regarded as lower limits only. In a waveform modelling study employing both regional and teleseismic waves, Song et al. (2009) were able to place tighter constraints on LVZ properties below south-central Mexico. Their models set LVZ thickness to vary between 3 and 5 km, with *S*-velocities between 2.0 and 2.7 km/s and *S*-velocity contrasts of 26–40% with surroundings. These values closely match those determined for Cascadia by Hansen et al. (2012).

LVZ thicknesses and *P*-velocities can also be constrained using dispersion of guided *P*-waves. These waves are generated within or in close proximity to the LVZ, with higher frequency waves guided within the LVZ propagating more slowly than lower frequency waves that are influenced by higher velocity surrounding material (see Fig. 2d). Since the guided phases propagate many wavelengths through the LVZ, they constrain average physical properties. In two compilation studies involving the 7 subduction zones listed in Section 4.1, Abers (2000, 2005) estimated the LVZ thickness to fall between 1–7 km and 2–8 km, respectively. These values average significantly lower than that for typical oceanic crust and are consistent with thicknesses reported for the LVZ in Cascadia (Audet et al., 2009; Hansen et al., 2012). It should also be noted, however, that there is at least one example of LVZ with thickness almost certainly greater than 10 km, in the Alaskan subduction zone (e.g. Ferris et al., 2003; Rondenay et al., 2008, see Fig. 8). In this instance, the associated crustal layer is thought to represent a subducted oceanic plateau possibly associated with the Yakutat terrane located immediately offshore.

Despite the fact that LVZ thickness and Poisson's ratio in subduction zones globally have not been simultaneously analysed in the same level of detail as Cascadia, we note that there is evidence to suggest that LVZ Poisson's ratios are generally high and that LVZ thickness is distinctly thinner than normal oceanic crust across a range of locations. Both tendencies are consistent with the current model, namely that the LVZ is an overpressured, metabasaltic Layer 2 constituting the upper oceanic crust.

4.3. LVZ depth extent

Although LVZs appear to be a ubiquitous feature of subduction zones, their expression in depth varies significantly (see Figs. 5 and 8). It has been widely noted that the depth at which the LVZ begins to fade depends on ambient thermal regime. In cold subduction zones, such as Alaska, northern Chile and Honshu, the seismic expression starts to disappear at depths between 80 and 120 km, whereas in warm subduction zones this depth is shallower, near 45 km in Cascadia and Nankai. This behaviour is neatly explained by appealing to thermal/petrologic models of slab metamorphism (Peacock and Wang, 1999; Hacker et al., 2003b). The eclogite facies boundary forms an "L" in P-T space, such that at low temperatures and high pressures, the boundary is approximately isothermal whereas at low pressures and high temperatures it is closer to isobaric. Thermal profiles of cold slabs intersect the facies boundaries at pressures starting near 3 GPa (90 km) whereas warmer slabs transform to eclogite at lower pressures near 1.3 GPa corresponding to depths near 40 km. These pressures/depths correspond well with observations of initiation of LVZ extinction. Moreover, the observation that the signature tends to fade from top to bottom is expected on the basis of thermal gradients and reaction kinetics; more specifically, eclogitization should proceed more rapidly in fine-grained, hydrated basalt of upper oceanic crust relative to coarse-grained, dry gabbro below.

The general correspondence between predictions from thermo-petrologic modelling of eclogitization and the well defined behaviour of LVZ extinction observed from seismic studies provides compelling support for the current model. It is rather more difficult to envisage how such behaviour with depth might be accommodated in models where the LVZ is ascribed solely to underthrust sediments.

4.4. Forearc mantle wedge

Although LVZs appear to be represented in all subduction zones, the absence of forearc Moho within the overriding plate does not share the same ubiquity. The extensively documented occurrence of this feature throughout Cascadia is not fully replicated, for example, in southwest Japan, Cascadia's closest thermal analogue. Receiver function studies by Shiomi et al. (2004) across the Chugoku–Shikoku region and Kato et al. (2010) across the Tokai district reveal the persistence of a normal polarity, island arc Moho right to the mantle wedge corner, indicating that serpentinization/hydration must be less pervasive there than in Cascadia. Heading south, Abe et al. (2011) document the presence of an inverted continental Moho beneath Kyushu, and high Poisson's ratio anomalies within mantle wedge above the Philippine Sea plate in the Ryukyu subduction zone (Chou et al., 2009) also point to high degrees of mantle serpentinization. Likewise, in the Kanto district, Kamiya and Kobayashi (2000) have interpreted high Poisson's ratio anomalies in the mantle wedge above the Philippine Sea plate as caused by serpentinization.

In the cold subduction regime of northeast Japan, the continental Moho imaged by receiver functions is observed to fade seaward of the arc (Kawakatsu and Watada, 2007, their Fig. 1B) suggesting pervasive serpentinization. Moreover, the development of a second, low velocity, high Poisson's ratio layer, lying immediately above the LVZ at depths of >80 km and independently imaged using regional tomography (Tsuji et al., 2008), has been interpreted to represent a layer of serpentinite transporting water into the deep mantle (Kawakatsu and Watada, 2007).

Other regions where significant forearc mantle serpentinization has been inferred either through aberrant overlying Moho's or Poisson's ratio anomalies include, Costa Rica (DeShon and Schwartz,

2004), northern Chile (Graeber and Asch, 1999; Sodoudi et al., 2011), the Marianas (Tibi et al., 2008) and Greece (Li et al., 2003; Sodoudi et al., 2006). The variability in signatures described above suggests that hydration of the forearc mantle wedge, though widespread, varies in degree, due presumably to some combination of water budget and thermal state of the incoming plate, and permeability structure at the plate interface.

5. Discussion and concluding remarks

In the preceding section, we have noted that descriptions of LVZs observed in subduction zones globally are generally consistent with the current model that identifies them with overpressured, upper oceanic crust. A consequence of this interpretation is that the oceanic Moho, possessing a more subtle seismic expression, has been frequently overlooked, at least in studies employing scattered waves. The process of dehydration that leads to the gradual disappearance of LVZs and the associated liberation of fluids into the mantle wedge also contributes in many instances to a reduction or even inversion in the seismic contrast at the Moho of the overriding plate. Hence, the LVZ serves to diminish the expression of both Mohos, albeit in different ways.

A number of additional implications of the current model warrant discussion. Hacker et al. (2003a,b) noted the importance of a structurally layered and variably hydrated oceanic crust in their comprehensive analysis of the petrology, elasticity and seismicity of subducting plates. One factor that was not explicitly accounted for, however, was the effect of pore pressure on seismic velocities which, as shown by Christensen (1984), can significantly outweigh effects due to mineralogy. Consequently, the interpretation of velocity models in terms of mineral composite elasticity calculations, metamorphic reactions and seismicity must proceed with caution and may need to be reviewed in instances where high pore fluid pressures are suspected.

The current model harbours some interesting implications for the relation between seismogenesis and structure. As an example, consider shallow slab seismicity in the sister (warm) subduction zones of Cascadia and Nankai. In both instances LVZs exhibiting high Vp/Vs ratios (and, by inference, high pore fluid pressures) are observed (Audet et al., 2009; Kodaira et al., 2004; Shelly et al., 2006). In Nankai, high resolution earthquake locations place regular Wadati–Benioff seismicity at the base of the LVZ whereas low-frequency earthquakes that constitute non-volcanic tremor fall on its upper boundary near 30 km depth. This latter association is consistent with the interpretation that the top of LVZ represent the plate boundary and that non-volcanic tremor is the high-frequency manifestation of slow-slip occurring on that interface (Ide et al., 2007). The interior of the LVZ appears to be devoid of seismicity suggesting that Wadati–Benioff events are restricted to the gabbroic, lower oceanic crust and underlying mantle. A parallel picture appears to be emerging for Cascadia. Although the precise depth range of tremor and low frequency earthquakes in Cascadia has been a matter of contention, there is growing consensus that, as in Nankai, it lies on a near-planar interface inferred to be the plate boundary (Brown et al., 2009; La Rocca et al., 2009, see Fig. 6). Even in those studies advocating a broader depth distribution of tremor (e.g., Kao et al., 2005), the peak of the distribution roughly coincides with the LVZ/E-layer. In contrast, Wadati–Benioff seismicity in the vicinity of Vancouver Island is located well below the LVZ/E-layer (Cassidy and Waldhauser, 2003; Kao et al., 2005).

These observations in Nankai and northern Cascadia prompt speculation as to whether high pore fluid pressures, while conducive to genesis of slow slip (Segall et al., 2010), discourage brittle failure within the subducting upper oceanic crust, at least in warm subduction zones at pressures below those associated with the basalt to eclogite transition. At first glance, this conjecture may seem counter-intuitive given that high pore pressures are an essential element of dehydration embrittlement, the mechanism widely favoured as responsible for intermediate depth seismicity (e.g., Raleigh and Paterson, 1965; Kirby et al., 1996; Hacker et al., 2003b). It is possible to envisage that pervasively hydrated and highly overpressured, fine-grained, upper oceanic crust (±overlying sediments) behaves in a more viscous manner than either the overriding plate or the underlying gabbroic layer (e.g., Fagereng & Sibson, 2010), perhaps through hydrolytic weakening (Griggs, 1967). That is, we may distinguish between i) steady state, high pore fluid pressures that impart a viscous rheology to metabasalt and so inhibit velocity weakening behaviour, and ii) transient, high-pore fluid pressures generated at the time of metamorphic reaction in better drained or drier circumstances that serve to, locally, reduce effective pressures and allow faulting via dehydration embrittlement to occur. Studies (Angiboust and Agard, 2010; Angiboust et al., 2011) of once subducted ophiolites exhumed within the Alpine orogeny provide geological support for these conjectures. Eclogitized metabasalt shows evidence of a once extensive hydration and more pronounced and pervasive ductile deformation than underlying metagabbros. Further testing of these ideas and improved understanding of the relations between seismicity, structure and metamorphism constitute fruitful ground for future research.

Acknowledgements

I am indebted to former students Stéphane Rondenay, Pascal Audet and Ralf Hansen, and colleagues Nik Christensen, Simon Peacock and Roy Hyndman for their integral contributions to the synthesis of shallow subduction zone structure presented here. Xiaohui Yuan and an anonymous referee provided constructive criticism that improved the presentation of this material. This research was supported by NSERC Discovery Grant RGPIN 138004.

References

Abe, Y., Ohkura, T., Hirahara, K., Shibutani, T., 2011. Water transportation through the Philippine Sea slab subducting beneath the central Kyushu region, Japan, as derived from receiver function analyses. Geophysical Research Letters 38 (L23305), http://dx.doi.org/10.1029/2011GL049688.

Abers, G.A., 2000. Hydrated subducted oceanic crust at 100–250 km depth. Earth and Planetary Science Letters 176, 323–330.

Abers, G.A., 2005. Seismic low-velocity layer at the top of subducting slabs: observations, predictions, and systematics. Physics of the Earth and Planetary Interiors 149, 7–29, http://dx.doi.org/10.1016/j.pepi.2004.10.002.

Abers, G.A., MacKenzie, L.S., Rondenay, S., Zhang, Z., Wech, A.G., Creager, K.C., 2009. Imaging the source region of Cascadia tremor and intermediate depth earthquakes. Geology 37, 1119–1122, http://dx.doi.org/10.1130/G30143A.1.

Agostinetti, N.P., Steckler, M.S., Lucente, F.P., 2009. Imaging the subducted slab under the Calabrian Arc, Italy, from receiver function analysis. Lithosphere 1, 131–138, http://dx.doi.org/10.1130/L49.1.

Angiboust, S., Agard, P., 2010. Initial water budget: the key to detaching large volumes of eclogitized oceanic crust along the subduction channel? Lithos 120, http://dx.doi.org/10.1016/j.lithos.2010.09.007.

Angiboust, S., Agard, P., Raimbourg, H., Yamato, P., Huet, B., 2011. Subduction interface processes recorded by eclogite-facies shear zones (Monviso, W. Alps). Lithos 127, 222–238, http://dx.doi.org/10.1016/j.lithos.2011.09.004.

Audet, P., Bostock, M.G., Boyarko, D.C., Brudzinski, M.R., Allen, R.M., 2010. Slab morphology in the Cascadia forearc and its relation to episodic tremor and slip. Journal of Geophysical Research 115 (B00A16), http://dx.doi.org/10.1029/2008JB006053.

Audet, P., Bostock, M.G., Christensen, N.I., Peacock, S.M., 2009. Seismic evidence for overpressured subducted oceanic crust and megathrust fault sealing. Nature 457, 76–78.

Audet, P., Bostock, M.G., Mercier, J.-P., Cassidy, J.F., 2008. Morphology of the Explorer/Juan de Fuca slab edge in northern Cascadia: imaging plate capture at a ridge-trench-transform triple junction. Geology 36, 895–898, http://dx.doi.org/10.1130/G25356A.

Blakely, R.J., Brocher, T.M., Wells, R.E., 2005. Subduction zone magnetic anomalies and implications for hydrated forearc mantle. Geology 33, 445–448.

Bostock, M.G., Hyndman, R.D., Rondenay, S., Peacock, S.M., 2002. An inverted continental Moho and serpentinization of the forearc mantle. Nature 417, 536–538.

Bostock, M.G., VanDecar, J.C., 1995. Upper mantle structure of the northern Cascadia subduction zone. Canadian Journal of Earth Sciences 32, 1–12.

Boyd, O.S., Savage, M.K., Sheehan, A.F., Jones, C.H., 2007. Illuminating the plate interface structure beneath Cook Strait, New Zealand, with receiver functions. Journal of Geophysical Research 112 (B06310), http://dx.doi.org/10.1029/2006JB004552.

Brocher, T.M., Parsons, T., Tréhu, A.M., Snelson, C.M., Fisher, M.A., 2003. Seismic evidence for widespread serpentinized forearc upper mantle along the Cascadia margin. Geology 31, 267–270.

Brown, E.H., Wilson, D.L., Armstrong, R.L., Harakal, J.E., 1982. Petrologic, structural, and age relations of serpentinite, amphibolite, and blueschist in the Shuksan Suite of Iron Mountain–Gee Point area, North Cascades, Washington. Geological Society of America Bulletin 93, 1087–1098.

Brown, J.R., Beroza, G.C., Ide, S., Ohta, K., Shelly, D.R., Schwartz, S.Y., Rabbel, W., Thorwart, M., Kao, H., 2009. Deep low frequency earthquakes in tremor localize to the plate interface in multiple subduction zones. Geophysical Research Letters 36 (L19306), http://dx.doi.org/10.1029/2009GL040027.

Calvert, A.J., Clowes, R.M., 1990. Deep, high-amplitude reflections from a major shear zone above the subducting Juan de Fuca plate. Geology 18, 1091–1094.

Calvert, A.J., Preston, L.A., Farahbod, A.M., 2011. Sedimentary underplating at the Cascadia mantle-wedge corner revealed by seismic imaging. Nature Geoscience 4, 545–548.

Calvert, A.J., Ramachandran, K., Kao, H., Fisher, M.A., 2006. Local thickening of the Cascadia forearc crust and the origin of seismic reflectors in the uppermost mantle. Tectonophysics 420, 175–188.

Cassidy, J.F., Ellis, R.M., 1993. S-wave velocity structure of the northern Cascadia subduction zone. Journal of Geophysical Research 98, 4407–4421.

Cassidy, J.F., Waldhauser, F., 2003. Evidence for both crustal and mantle earthquakes in the subducting Juan de Fuca plate. Geophysical Research Letters 30 (1095), http://dx.doi.org/10.1029/2002GL015511.

Chou, H.-C., Kuo, B.-Y., Chiao, L.-Y., Zhao, D., Hung, S.-H., 2009. Tomography of the westernmost Ryukyu subduction zone and the serpentinization of the fore-arc mantle. Journal of Geophysical Research 114 (B12301), http://dx.doi.org/10.1029/2008JB006192.

Christensen, N.I., 1978. Ophiolites, seismic velocities and oceanic crustal structure. Tectonophysics 47, 131–157.

Christensen, N.I., 1984. Pore pressure and oceanic crustal seismic structure. Geophysical Journal of the Royal Astronomical Society 79, 411–423.

Christensen, N.I., 1996. Poisson's ratio and crustal seismology. Journal of Geophysical Research 101, 3139–3156.

Christensen, N.I., 2004. Serpentines, peridotites and seismology. International Geology Review 46, 795–816.

Christensen, N.I., Salisbury, M.H., 1975. Structure and constitution of the lower oceanic crust. Reviews of Geophysics and Space Physics 13, 57–86.

Clowes, R.M., Brandon, M.T., Green, A.G., Yorath, C.J., Sutherland Brown, A., Kanasewich, E.R., Spencer, C., 1987a. LITHOPROBE southern Vancouver Island: Cenozoic subduction complex imaged by deep seismic reflections. Canadian Journal of Earth Sciences 24, 31–51.

Clowes, R.M., Yorath, C.J., Hyndman, R.D., 1987b. Reflection mapping across the convergent margin of western Canada. Geophysical Journal of the Royal Astronomical Society 89, 79–84.

Coleman, R.G., 1971. Petrologic and geophysical nature of serpentinites. Geological Society of America Bulletin 82, 897–918.

DeShon, H.R., Schwartz, S.Y., 2004. Evidence for serpentinization of the forearc mantle wedge along the Nicoya Peninsula, Costa Rica. Geophysical Research Letters 31 (L21611), http://dx.doi.org/10.1029/2004GL021179.

Fagereng, A., Sibson, R.H., 2010. Melange rheology and seismic style. Geology 38 (8), 751–754, http://dx.doi.org/10.1130/G30868.1.

Ferris, A., Abers, G.A., Christensen, D.H., Veenstra, E., 2003. High resolution image of the subducted Pacific (?) plate beneath Central Alaska, 50–150 km depth. Earth and Planetary Science Letters 214, 575–588.

Fisher, A.T., 1998. Permeability within basaltic oceanic crust. Reviews of Geophysics 36, 143–182.

Fyfe, W.S., Price, N.J., Thompson, A.B., 1978. Fluids in the Earth's Crust. Elsevier, New York.

Gerver, M., Markushevitch, V., 1966. Determination of a seismic wave velocity from the travel time curve. Geophysical Journal of the Royal Astronomical Society 11, 165–173.

Graeber, F.M., Asch, G., 1999. Three-dimensional models of *P* wave velocity and *P*-to-*S* velocity ratio in the southern central Andes by simultaneous inversion of local earthquake data. Journal of Geophysical Research 104 (B9), 20,237–20,256.

Green, A.G., Clowes, R.M., Yorath, C.J., Spencer, C., Kanasewich, E.R., Brandon, M.T., Sutherland Brown, A., 1986. Seismic reflection imaging of the Juan de Fuca plate. Nature 319, 210–213.

Griggs, D., 1967. Hydrolytic weakening of quartz and other silicates. Geophysical Journal of the Royal Astronomical Society 14, 19–31, http://dx.doi.org/10.1111/j.1365-246X.1967.tb06218.x.

Gross, K., Micksch, U., TIPTEQ Research Group, 2008. The reflection seismic survey of project TIPTEQ—the inventory of the Chilean subduction zone at 38.2S. Geophysical Journal International, http://dx.doi.org/10.1111/j.1365-246X.2007.03680.

Hacker, B.R., 1996. Eclogite formation and the rheology, buoyancy, seismicity, and H2O content of oceanic crust. In: Bebout, G.E., et al. (Ed.), Dynamics of Subduction. AGU, Washington, D. C., pp. 337–346. 1996.

Hacker, B.R., Abers, G.A., Peacock, S.M., 2003a. Subduction factory 1. Theoretical mineralogy, densities, seismic wave speeds, and H2O contents. Journal of Geophysical Research 108 (2029), http://dx.doi.org/10.1029/2001JB001127.

Hacker, B.R., Peacock, S.M., Abers, G.A., Holloway, S.D., 2003b. Subduction factory 2. Are intermediate-depth earthquakes in subducting slabs linked to metamorphic dehydration reactions? Journal of Geophysical Research 108 (2030), http://dx.doi.org/10.1029/2001JB001129.

Hansen, R.T.J., Bostock, M.G., Christensen, N.I., 2012. Nature of the low velocity zone in Cascadia from receiver function waveform inversion. Earth and Planetary Science Letters 337–338, 25–38, http://dx.doi.org/10.1016/j.epsl.2012.05.031.

Hyndman, R.D., 1988. Dipping seismic reflectors, electrically conductive zones and trapped water in the crust over a conducting plate. Journal of Geophysical Research 93, 13391–13405.

Hyndman, R.D., Peacock, S.M., 2003. Serpentinization of the forearc mantle. Earth and Planetary Science Letters 212, 417–432.

Hyndman, R.D., Yorath, C.J., Clowes, R.M., Davis, E.E., 1990. The northern Cascadia subduction zone at Vancouver Island: seismic structure and tectonic history. Canadian Journal of Earth Sciences 27, 313–329.

Ide, S., Shelly, D.R., Beroza, G.C., 2007. The mechanism of deep low frequency earthquakes: further evidence that deep non-volcanic tremor is generated by shear slip on the plate interface. Geophysical Research Letters 34 (L03308), http://dx.doi.org/10.1029/2006GL028890.

Jödicke, H., Jording, A., Ferrari, L., Arzate, J., Mezger, K., Rüpke, L., 2006. Fluid release from the subducted Cocos plate and partial melting of the crust deduced from magnetotelluric studies in southern Mexico: implications for the generation of volcanism and subduction dynamics. Journal of Geophysical Research 111 (B08102), http://dx.doi.org/10.1029/2005JB003739.

Kamiya, S., Kobayashi, Y., 2000. Seismological evidence for the existence of serpentinized wedge mantle. Geophysical Research Letters 27, 819–822.

Kao, H., Shan, S.-J., Dragert, H., Rogers, G., Cassidy, J.F., Ramachandran, K., 2005. A wide depth distribution of seismic tremors along the northern Cascadia margin. Nature 436, 841–844, http://dx.doi.org/10.1038/nature03903.

Kato, A., Iidaka, T., Ikuta, R., Yoshida, Y., Katsumata, K., Iwasaki, T., Sakai, S.I., Thurber, C., Tsumura, N., Yamaoka, K., Watan- abe, T., Kunitomo, T., Yamazaki, F., Okubo, M., Suzuki, S., Hi- rata, N., 2010. Variations of fluid pressure within the subducting oceanic crust and slow earthquakes. Geophysical Research Letters 37 (L14310), http://dx.doi.org/10.1029/2010GL043723.

Kawakatsu, H., Watada, S., 2007. Seismic evidence for deep-water transportation in the mantle. Science 316, 1468–1471.

Kern, H., 1993. P and S-wave anisotropy and shear-wave splitting at pressure and temperature in possible mantle rocks and their relation to the rock fabric. Physics of the Earth and Planetary Interiors 78, 245–256.

Kim, Y., Clayton, R.W., Jackson, J.M., 2010. Geometry and seismic properties of the subducting Cocos plate in Central Mexico. Journal of Geophysical Research 115, http://dx.doi.org/10.1029/2009JB006942.

Kim, Y., Clayton, R.W., Keppie, F., 2011. Evidence of a collision between the Yucatan Block and Mexico in the Miocene. Geophysical Journal International, http://dx.doi.org/10.1111/j.1365-246X.2011.05191.x.

Kim, Y., Miller, M.S., Pearce, F.D., Clayton, R., in press. Seismic imaging of the Cocos plate subduction zone system in central Mexico. Geochemistry, Geophysics, Geosystems, http://dx.doi.org/10.1029/2012GC004033.

Kirby, S., Engdahl, E.R., Denlinger, R., 1996. Intermediate-depth intraslab earthquakes and arc volcanism as physical expressions of crustal and uppermost mantle metamorphism in subducting slabs. In: Bebout, G.E., et al. (Ed.), Subduction: Top to Bottom. : Geophys. Monogr. Ser., vol. 96. AGU, Washington, D. C., pp. 195–214.

Kodaira, S., Iidaka, T., Kato, A., Park, J., Iwasaki, T., Kaneda, Y., 2004. High pore fluid pressure may cause silent slip in the Nankai Trough. Science 304, 1295–1298.

Kurtz, R.D., DeLaurier, J.M., Gupta, J.C., 1990. The electrical conductivity distribution beneath Vancouver Island: a region of active plate subduction. Journal of Geophysical Research 95, 10929–10946.

Langston, C.A., 1977. Corvallis, Oregon, crustal and upper mantle receiver structure from teleseismic *P* and *S* waves. Bulletin of the Seismological Society of America 67, 713–724.

Langston, C.A., 1981. Evidence for the subducting lithosphere under southern Vancouver Island and western Oregon from teleseismic P wave conversion. Journal of Geophysical Research 86, 3857–3866.

La Rocca, M., Creager, K.C., Galluzzo, D., Malone, S., Vidale, J.E., Sweet, J.R., Wech, A.G., 2009. Cascadia tremor located near plate interface constrained by S minus P wave times. Science 323, 620–623, http://dx.doi.org/10.1126/science.1167112.

Li, X., Bock, G., Vafidis, A., Kind, R., Harjes, H.-P., Hanka, W., Wylegalla, K., Meijde, M.v.d., Yuan, X., 2003. Receiver function study of the Hellenic subduction zone: imaging crustal thickness variations and the oceanic Moho of the descending African lithosphere. Geophysical Journal International 155 (2), 733–748, http://dx.doi.org/10.1046/j.1365-246X.2003.02100.x.

McGary, R.S., Rondenay, S., Evans, R.L., Abers, G.A., Wannamaker, P.E., 2011. A joint geophysical investigation of the Cascadia subduction system in central Washington using dense arrays of passive seismic and magnetotelluric station data. Abstract V54B-03 presented at the 2011 Fall Mtg, AGU San Francisco, Calif. 5–9 Dec.

MacKenzie, L.S., Abers, G.A., Rondenay, S., Fischer, K.M., 2010. Imaging a steeply dipping subducting slab in southern Central America. Earth and Planetary Science Letters 296, 459–468.

Martin, S., Rietbrock, A., Haberland, C., Asch, G., 2003. Guided waves propagating in subducted oceanic crust. Journal of Geophysical Research 108, http://dx.doi.org/10.1029/2003JB002450.

Michaelson, C.A., Weaver, C.S., 1986. Upper mantle structure from teleseismic P arrivals in Washington and northern Oregon. Journal of Geophysical Research 91, 2077–2094.

Nabelek, J., Trehu, A., Li, X.Q., Fabritius, A., 1996. Lithospheric structure of the Cascadia Arc beneath Oregon. Eos Trans. AGU, 1996 Fall Meeting Suppl. Abstract T72B-10.

Nedimovic, M.R., Bohnenstiehl, D.R., Carbotte, S.M., Canales, J.P., Dziak, R.P., 2009. Faulting and hydration of the Juan de Fuca plate system. Earth and Planetary Science Letters 284, 94–102.

Nedimovic, M.R., Hyndman, R.D., Ramachandran, K., Spence, G.D., 2003. Reflection signature of seismic and aseismic slip on the northern Cascadia subduction interface. Nature 424, 416–420.

Nicholson, T., Bostock, M.G., Cassidy, J.F., 2005. New constraints on subduction zone structure in northern Cascadia. Geophysical Journal International 161, 849–859.

Nikulin, A., Levin, A., Park, J., 2009. Receiver function study of the Cascadia megathrust: evidence for localized serpentinization. Geochemistry, Geophysics, Geosystems 10 (Q07004), http://dx.doi.org/10.1029/2009/GC002376.

Obrebski, M., Allen, R.M., Xue, M., Hung, S.-H., 2010. Slab-plume interaction beneath the Pacific Northwest. Geophysical Research Letters 37 (L14305), http://dx.doi.org/10.1029/2010GL043489.

Oncken, O., the ANCORP working group, 1999. Seismic reflection image revealing offset of Andean subduction-zone earthquake locations into oceanic mantle. Nature 397, 341–344.

Park, J., Yuan, H., Levin, V., 2004. Subduction zone anisotropy beneath Corvallis, Oregon: a serpentinite skid mark of trench-parallel terrane migration? Journal of Geophysical Research 109 (B10306), http://dx.doi.org/10.1029/2003JB002718.

Parsons, T., Trehu, A.M., Luetgert, J.H., Miller, K., Killbride, F., Wells, R.E., Fisher, M.A., Flueh, E., ten Brink, U.S., Christensen, N.I., 1998. A new view into the Cascadia subduction zone and volcanic arc: implications for earthquake hazards along the Washington margin. Geology 26, 199–201.

Peacock, S.M., 1987. Serpentinization and infiltration metasomatism in the Trinity peridotite, Klamath province, northern California; implications for subduction zones. Contributions to Mineralogy and Petrology 95, 55–70.

Peacock, S.M., 2001. Are the lower planes of double seismic zones caused by serpentine dehydration in subducting oceanic mantle? Geology 29, 299–302.

Peacock, S.M., Christensen, N.I., Bostock, M.G., Audet, P., 2011. High pore pressures and porosity at 35 km depth in the Cascadia subduction zone. Geology 39, 471–474, http://dx.doi.org/10.1130/G31649.1.

Peacock, S.M., Hyndman, R.D., 1999. Hydrous minerals in the mantle wedge and the maximum depth of subduction thrust earthquakes. Geophysical Research Letters 26, 2517–2520.

Peacock, S.M., Wang, K., 1999. Seismic consequences of warm versus cool subduction metamorphism: examples from southwest and northeast Japan. Science 286, 937–939.

Pearce, F.D., Rondenay, S., Sachpazi, M., Charalampakis, M., Royden, L.H., 2012. Seismic investigation of the transition from continental to oceanic subduction along the western Hellenic subduction zone. Journal of Geophysical Research 117, B07306, http://dx.doi.org/10.1029/2011JB009023.

Preston, L.A., Creager, K.C., Crosson, R.S., Brocher, T.M., Tréhu, A.M., 2003. Intraslab earthquakes: dehydration of the Cascadia slab. Science 302, 1197–1200.

Raitt, R.W., 1963. The crustal rocks. In: Hill, M.N. (Ed.), The Sea, vol. 3. Interscience Publ., New York-London, pp. 85–102.

Raleigh, C.B., Paterson, M.S., 1965. Experimental deformation of serpentine and its tectonic implications. Geophysical Journal of the Royal Astronomical Society 14, 113–118.

Ramachandran, K., Hyndman, R.D., Brocher, T.M., 2006. Regional P wave velocity structure of the Northern Cascadia subduction zone. Journal of Geophysical Research 111 (B12301), http://dx.doi.org/10.1029/2005JB004108.

Rasmussen, J., Humphreys, E., 1988. Tomographic image of the Juan de Fuca plate beneath Washington and western Oregon using teleseismic P-wave travel times. Geophysical Research Letters 15, 1417–1420.

Rea, D.K., Ruff, L.J., 1996. Composition and mass flux of sediment entering the worlds subduction zones: implications for global sediment budgets, great earthquakes, and volcanism. Earth and Planetary Science Letters 140, 1–12.

Rohr, K.M.M., 1994. Increase of seismic velocities in upper oceanic crust and hydrothermal circulation in the Juan de Fuca plate. Geophysical Research Letters 21, 2163–2166.

Rondenay, S., Abers, G.A., van Keken, P.E., 2008. Seismic imaging of subduction zone metamorphism. Geology 36, 275–278.

Rondenay, S., Bostock, M.G., Shragge, J., 2001. Multiparameter two-dimensional inversion of scattered teleseismic body waves: 3—application to the Cascadia 1993 data set. Journal of Geophysical Research 106, 30795–30807.

Saad, A.F., 1969. Magnetic properties of ultramafic rocks from Red Mountain, California. Geophysics 34, 974–987.

Salisbury, M.H., Christensen, N.I., 1978. The seismic velocity structure of a traverse through the Bay of Islands ophiolite complex, Newfoundland, an exposure of oceanic crust and upper mantle. Journal of Geophysical Research 83, 805–817.

Salisbury, M.H., Christensen, N.I., Vine, F.J., Smith, G.C., Eleftheriou, S., 1989. Geophysical structure of the Troodos Ophiolite from downhole logging. In: Gibson, I.L., Malpas, J., Robinson, P.T., Xenophontos, C. (Eds.), Cyprus Crustal Study Project: Initial Report, Hole CY-4. Geological Survey of Canada, Ottawa, Ontario, Canada, pp. 331–349.

Schmandt, B., Humphreys, E., 2011. Seismically imaged relict slab from the 55 Ma Siletzia accretion to the northwest United States. Geology 39, 175–178, http://dx.doi.org/10.1130/G31558.

Segall, P., Rubin, A.M., Bradley, A.M., Rice, J.R., 2010. Dilatant strengthening as a mechanism for slow slip events. Journal of Geophysical Research 115 (B12305), http://dx.doi.org/10.1029/2010JB007449.

Shelly, D.R., Beroza, G.C., Ide, S., Nakamura, S., 2006. Low-frequency earthquakes in Shikoku, Japan, and their relationship to episodic tremor and slip. Nature 442, 188–191.

Shiomi, K., Matsubara, M., Ito, Y., Obara, K., 2008. Simple relationship between seismic activity along Philippine Sea slab and geometry of oceanic Moho beneath southwest Japan (/it) Geophysical Journal International 173, 1018–1029.

Shiomi, K., Sato, H., Obara, K., Ohtake, M., 2004. Configuration of subducting Philippine Sea plate beneath southwest Japan revealed from receiver function analysis based on the multivariate autoregressive model. Journal of Geophysical Research 109 (B04308), http://dx.doi.org/10.1029/2003JB002774.

Sodoudi, F., Kind, R., Hatzfeld, D., Priestley, K., Hanka, W., Wylegalla, K., Stavrakakis, G., Vafidis, A., Harjes, H.-P., Bohnhoff, M., 2006. Lithospheric structure of the Aegean obtained from P and S receiver functions. Journal of Geophysical Research 111 (B12307), http://dx.doi.org/10.1029/2005JB003932.

Sodoudi, F., Yuan, X., Asch, G., Kind, R., 2011. High-resolution image of the geometry and thickness of the subducting Nazca lithosphere beneath northern Chile. Journal of Geophysical Research 116 (B04302), http://dx.doi.org/10.1029/2010JB007829.

Song, T.-R., Helmberger, D.V., 2007. Validating tomography with broadband waveform modeling: An example at La Ristra Transect in the southwestern United States. Geophysical Journal International 171, 244–258.

Song, T.-R., Helmberger, D.V., Brudzinski, M.R., Clayton, R.W., Davis, P., Perez-Campos, X., Singh, S.K., 2009. Subducting slab ultra-slow layer coincident with silent earthquakes in southern Mexico. Science 324, 502–506, http://dx.doi.org/10.1126/science.1167595.

Soyer, W., Unsworth, M., 2006. Deep electrical structure of the northern Cascadia (British Columbia, Canada) subduction zone: implications for the distribution of fluids. Geology 34, 53–56, http://dx.doi.org/10.1130/G21951.1.

Suckale, J., Rondenay, S., Sachpazi, M., Charalampakis, M., Hosa, A., Royden, L.H., 2009. High-resolution seismic imaging of the western Hellenic subduction zone using teleseismic scattered waves. Geophysical Journal International 178, 775–791, http://dx.doi.org/10.1111/j.1365-246X.2009.04170.x.

Tibi, R., Wiens, D.A., Yuan, X., 2008. Seismic evidence for widespread serpentinized forearc mantle along the Mariana convergence margin. Geophysical Research Letters 35 (L13303), http://dx.doi.org/10.1029/2008GL034163.

Trehu, A.M., Asudeh, I., Brocher, T.M., Luetgert, J.H., Mooney, W.D., Nabelek, J.L., Nakamura, Y., 1994. Crustal architecture of the Cascadia forearc. Science 266, 237–242.

Tsuji, Y., Nakajima, J., Hasegawa, A., 2008. Tomographic evidence for hydrated oceanic crust of the Pacific slab beneath northeastern Japan: implications for water transportation in subduction zones. Geophysical Research Letters 35 (L14308), http://dx.doi.org/10.1029/2008GL034461.

Ulmer, P., Tromsdorff, V., 1995. Serpentine stability to mantle depths and subduction-related magmatism. Science 268, 858–861.

Wannamaker, P.E., Booker, J.R., Jones, A.G., Chave, A.D., Filloux, J.H., Waff, H.S., Law, L.K., 1989. Resistivity cross section through the Juan de Fuca subduction system and its tectonic implications. Journal of Geophysical Research 94, 14,127–14,144.

White, R.S., McKenzie, D., ONions, R.K., 1992. Oceanic thickness from seismic measurements and rare earth element inversions. Journal of Geophysical Research 97, 19683–19715.

Wielandt, E., 1987. On the validity of the ray approximation for interpreting delay times. In: Nolet, G. (Ed.), Seismic Tomography. Reidel, Holland, pp. 85–98.

Yuan, X., Sobolev, S.V., Kind, R., Oncken, O., Bock, G., Asch, G., Schurr, B., Graeber, F., Rudloff, A., Hanka, W., Wylegalla, K., Tibi, R., Haberland, C., Rietbock, A., Giese, P., Wigger, P., Röwer, P., Zandt, G., Beck, S., Wallace, T., Pardo, M., Comte, D., 2000. Subduction and collision processes in the Central Andes constrained by converted seismic phases. Nature 408, 958–961.

Zhang, H., Thurber, C.H., Shelly, D.R., Ide, S., Beroza, G.C., Hasegawa, A., 2004. High-resolution subducting-slab structure beneath northern Honshu, Japan, revealed by double-difference tomography. Geology 32, 361–364.

Zhao, D., Wang, K., Rogers, G.C., Peacock, S.M., 2001. Toographic image of low *P* velocity anomalies above slab in northern Cascadia subduction zone. Earth Planets Space 53, 285–293.

Zhu, L., Kanamori, H., 2000. Moho depth variation in southern California from teleseismic receiver functions. Journal of Geophysical Research 105, 2969–2980.